



ISSN: 0067-2904

# Heat Flux of Ionized Layers near the Cathode at Atmospheric Pressure in an Arc Discharge

### Tapark Abdlraheem Saber, Rafid Abbas Ali\*, Huda Muhammad Jawad

Department of physics, College science, Mustansiriyah University Baghdad, Iraq

Received: 5/11/2023 Accepted:21/8/2024 Published: 30/8/2025

#### Abstract

An arc discharge model for the discharge layers close to the cathode surface is reported. In addition to calculating the degree of plasma ionization and the ionization length to the average free path ratio; the effect of the voltage (U=10 V and 20 V), the temperature of the cathode surface, and mixture concentration (xenon-sodium) on the current density of plasma  $(j_p)$ , of ion  $(j_i)$ , of electrons  $(j_e)$ , and of electrons emitted from the surface cathode  $(j_{em})$ , the ion energy density qi and the electron energy  $q_e$  was determined. The voltage (U=20V) had a greater effect. At sodium concentrations between (0.1 and 0.5 moles) added to xenon, a shift towards lower temperatures (1500-3000) K after adding sodium concentrations (0.001, 0.01, 0.1 and 0.5) moles to xenon, especially at voltage U=20 V was noted. As a result of the increase in ionization processes, the collision and kinetic energy of electrons have a significant effect on increasing these coefficients at temperatures (3000-5000) K.

**Keywords:** arc discharge, electron, and ion current density, Ion energy, electron energy, plasma ionization degree.

## التدفق الحراري للطبقات المتأينة بالقرب من الكاثود عند الضغط الجوي في تفريغ القوس

تبارك عبد الرحيم صبر, رافد عباس علي \*. هدى محمد جواد قسم الفيزباء، كلية العلوم، الجامعة المستنصرية, بغداد، العراق

#### الخلاصه

تم دراسة نموذج التفريغ القوسي للطبقات المؤينة القريبة من سطح الكاثود لتحديد تأثير الجهد ودرجة حرارة سطح الكاثود وتركيزات خليط الزينون—الصوديوم على كثافة تيار البلازما والأيونات والإلكترونات المنبعثة من سطح الكاثود. تم تحديد الجهد U=10 فولت، U=10 فولت، ودرجة حرارة سطح الكاثود U=10 وخليط الزينون—الصوديوم) على U=10 أوكذلك على U=10 من خلال الدراسة، من الواضح أن الجهد U=10 فولت له تأثير أكبر من U=10 فولت ، وخاصة عند تركيزات ( U=10 مول. ومع التحول نحو درجات حرارة منخفضة (U=10 نتيجة لزيادة عمليات التأين والتصادم والطاقة الحركية الموديوم المضافه الى الزينون عند الجهد U=10 نتيجة لزيادة عمليات التأين والتصادم والطاقة الحركية للإلكترونات، كان لدرجات الحرارة U=10 ما ألمن الثير في زيادة هذه المعلمات.

\*Email: rafidphy 1972@uomustansiriyah.edu.iq

3223

\_\_\_

#### 1. Introduction

Plasma arc discharge is the process of creating plasma by passing an electric current through gas. This method involves the use of an electric arc, which is a continuous electrical discharge between two electrodes. The electrodes are often made of conductive materials such as metal [1, 2]. Two electrodes are placed in the chamber filled with a gas, which is often an inert gas such as argon or helium, and a potential difference (voltage) is applied between them. There is no significant ionization inside the discharge when very low voltage is used; however, as the voltage increases, it reaches a point where it ionizes the gas molecules. Ionization is the process of converting neutral atoms or molecules into charged ions by adding or removing electrons. In this case, electrons are stripped from the gas atoms, creating a mixture of positive ions and free electrons [3]. The ionization process results in the formation of an arc or plasma discharge. Electrically charged particles, including ions and electrons, form a plasma state of matter in which the gas is partially ionized, enabling it to conduct electricity [4]. Once the arc is created, a continuous flow of electric current through the ionized gas maintains the plasma. The high energy of the electrons in the arc causes them to collide with the gas molecules, maintaining the ionization and plasma state [5, 6]. Rego used arc discharge in optical fibers, such as the fiber connection in the core device [7]. Ghorui and Das used arc discharge to explore the arc instability in plasma jets using nonlinear dynamic approaches to obtain accurate structural descriptions of different locations within the flame [8]. Timofeev used an arc discharge device and a method using microwave plasma to generate an arc at low voltage, which reduces the wear of electrodes and increases the applicability of arc discharge technology in the biomedical field [9]. Jassam and Ali used dysprasium-doped arc cathodes which were used as a light source for a high-pressure xenon arc and greatly influenced the generation of optical radiation, resulting in radiation mostly in the visible, infrared or ultraviolet regions [10].

In this research, the arc discharge model (close to the cathode) was used to study the effect of cathode temperature (3000-5000) K at applied voltages of (U=10 and U=20) V and sodium concentrations of (0.001, 0.01, 0.1 and 0.5) mole added to xenon on different current densities  $(j_p, j_i \cdot j_e, \text{ and j})$ , different energy densities ( $q_e, q_i$ ,), ionization degree and ratio of free path length to ionization length ( $\alpha$ ).

#### 2. Model of arc discharge

A high-pressure arc discharge's thermal cathode model is considered. It is of two parts as depicted in Figure 1. The plasma arc is connected to the first part of the cathode surface, which is heated by a high-pressure arc discharge and the current is collected through arc discharge. The second component is the gas, after the gas is heated or emits radiation, the radiation energy is exchanged for a rise in the gas temperature. It is crucial to distinguish between the first portion linked to the plasma and the second portion correlating to the gas because the cathode substance is known for its thermal conductivity K = k (T) [11]. At the cathode surface, in the narrow plasma wave layer near the cathode, part of the energy from the plasma arc is collected due to its intensity [12]. The surface thermostat  $T_W$  and low voltage U in this layer affect the one-dimensional current transferred across it with a change in surface temperature  $T_W$ . The gas cathode's exchange temperature or the surface's vanished ray area that is connected to the gas will vary as in the given equations [13]:

$$q = q(T_w, u)$$
 Which is defining per  $(T_w \ge Tc)$ . (1)

$$j = j(T_w, u)$$
 Which is defining per  $(T_w \ge \text{Tc})$ . (2)

The cathode body's surface temperature distribution can be determined using the cathode body's thermal conductivity, which is represented by the equation in  $q(T_w, u)$  function [14]:

$$\nabla.\left(K\nabla_{T}\right) \tag{3}$$

Where: K is the thermal conductivity and  $\Delta_T$  is the change in temperature

The current flux density of the first and second sections is described by Equations (1) and (2). The temperature of the area inside the surface in contact with the plasma arc increases as (Tw) increases, and decreases as the surface section in contact with the gas is exposed

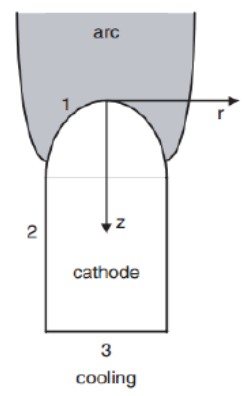


Figure 1: Thermal Cathode [10]

Unified modeling is used to perform calculations that require solving the one-dimensional equations of near-perfect neutrality, ionization equilibrium, and thermal equilibrium of the confined plasma charge (located on the cathode surface) taking into account the thermal emission of electrons. Since the particle (electron) moves from the cathode edge surface to the ionization layer, the determination of the ion density and electron current is possible. The ions as well as the electrons flow naturally towards the electrodes and the thickness of the space charge shell is much less than the ionization length on the cathode surface. When the influence of the electric field on the ionization layer is small, the electron currents move to the cathode edge. Since the cathode electrode requires high negativity, the strong electric current induces the ionization layer field to push the electrons, which rise to the top of the cathode. The equation for the ion current density is as follows [15]

$$j_i^0 = eD_{ia} \frac{nSaha}{d} \tag{4}$$

Where n is the number of electrons.

The electron current density at the electrode surface  $z(j_e^0)$  is:

$$j_e^0 = eD_{ea} \frac{nSaha}{d} \tag{5}$$

Where  $D_{ia}$  and  $D_{ea}$  are the coefficients regarding the spread of the electron and the ions, and d is the ionization duration.

In the absence of an electric field within the ionization layer, which is either repulsive or accelerating, the flow of electrons that might reach the edge sheath must be restricted. Since the majority of the cathode electric current (electron emission from the cathode surface) is transmitted, this explains why the phenomenon at the anode is mostly due to the magnetic field in the sheath and the ionization. Each of these processes (ionization, collisions, and emission) is associated with Schottky amplification of thermionic emission, a process that regulates the electron emitted under high-pressure arc conditions, such that each electron emits an energy equivalent to the cathode's work function. Since the electron emission causes the cathode to be quenched, a mechanism must be devised to overcome this quenching and achieve the temperatures required for thermionic emission at the cathode surface. A process

of this kind might work by heating the cathode with plasma ions and accelerating them within the space charge envelope. It is important that it be ionic, and that the cathode surface current is not too low. The cathode surface energy must balance [16]. such as:

$$\frac{j_i}{e}(e\ U_{sh} + Ai - Af) = \frac{j_{em}}{e}Af + q\tag{6}$$

Where:  $j_i$  is the ion current density on the surface of the cathode ,  $A_i$  is the gas's ionization energy generating the plasma ,  $j_{em}$  is the density of the emitted electrons,  $A_f$  is the effective work function, and  $U_{sh}$  is the sheath voltage.

The dependence of the plasma's energy transfer on the cathode surface at the local level on the lattice density is the decrease in near-cathode voltage U, which is evaluated by formulas (7,8, and 9). This is most important result for calculating the near-cathode layer computation, as shown by the following formulas:

$$q = q_p - q_r \tag{7}$$

$$q_{r=\epsilon\sigma T_{W}^{4}} \tag{8}$$

$$q_p = q_i + q_e - q_{em} (9)$$

Where:  $q_p$  is the energy flux density of the plasma,  $q_i$  is the thickness of ion energy flux,  $q_e$  is the plasma electrons' energy flow density,  $q_{em}$  is the energy flux density from electron emission,  $\varepsilon$  is the emissivity of the cathode substance, and  $\sigma$  is Stefan Boltzmann constant

Equations (6,7, and 8)'s second formula can also be expressed equivalently [18].

$$q_p = JU - j(Af + 3.2kT_e)/e$$
 (9)

Where:  $q_p$  is the plasma energy density,  $A_f$  is the effective work function,  $T_e$  is the electron temperature, K is the Boltzmann constant, e is the charge of electrons,  $U_i$  is the voltage of the layers near the cathode, and j is the current density.

The calculated difference between the electrical energy transferred by an electronic current from the layer to the combined plasma and the amount of electrical energy placed near the cathode for each layer unit area is represented in this equation (10) as the plasma-related energy is transferred to the cathode surface. The heat conduction equation controls the cathode's temperature distribution [19].

$$\rho c_p \frac{\partial \tau}{\partial t} = \nabla \cdot (K \nabla T) \tag{10}$$

Where: t is the time,  $\rho$  is the mass density,  $c_p$  is the specific heat, and k is the thermal conductivity of the cathode material.

The heat generated within the cathode by the Joule action, as explained above, was not taken into consideration by this calculation. Methods utilized in gas-metal arc simulations can be used to add an explanation of heat production within a cathode. For instance, the enthalpy technique is utilized as well as the effective specific heat technique that has been employed within the cathode. Equation (7) was resolved under the subsequent boundary conditions. Depending on the ionization and excitation processes that occur in the layers close to the cathode surface is the net energy's density, q, which contributes to the near-decrease in

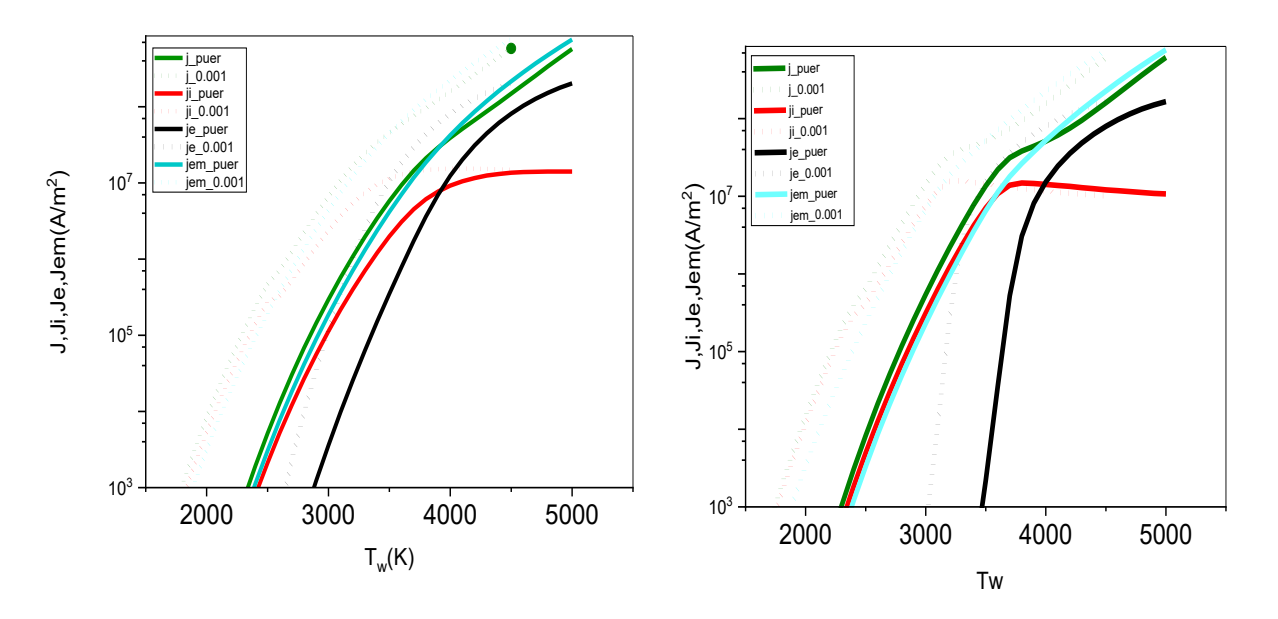
cathode at voltage and the local surface temperature Tw from the plasma to the cathode surface [20].

#### 3. Results and Discussion:

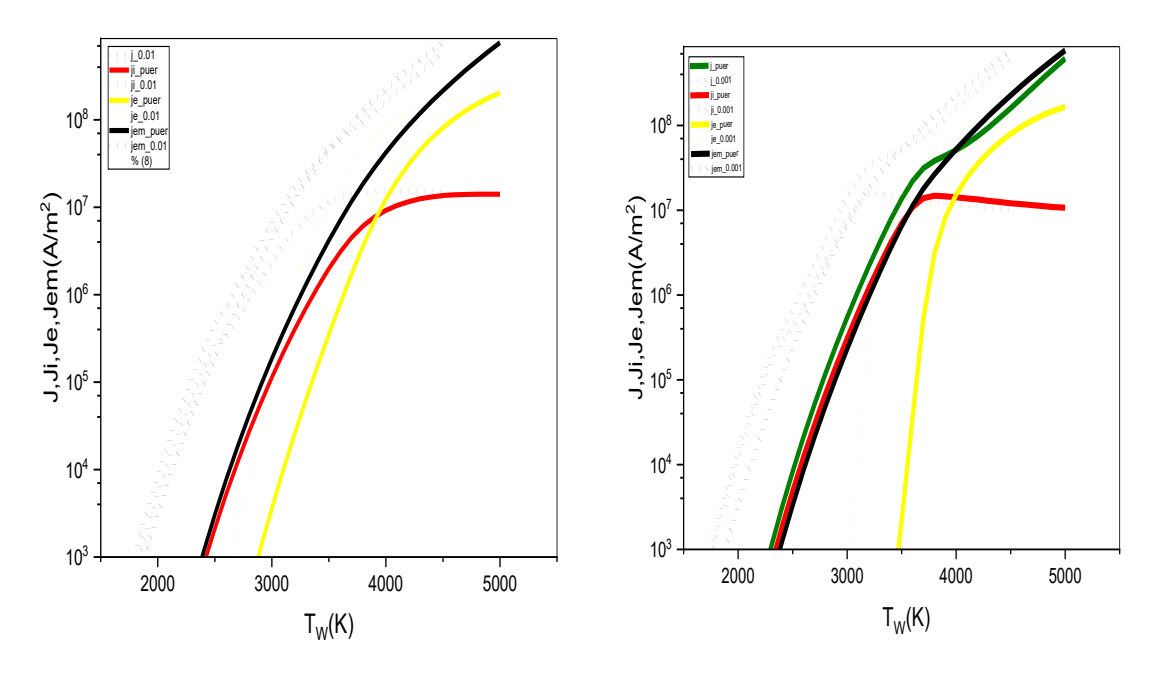
The relationship between plasma current density (j), electron current density  $(j_e)$ , ion current density  $(j_i)$  and cathode surface temperature (Tw) in Kelvin at voltages U=10V and U=20V for different sodium concentrations of (0.001, 0.01, 0.1 and 0.5) mole added to xenon is shown in Figures (1), (2), (3) and (4). The plasma current density (j) started to emit at a temperature between 2400 and 5000 K at U=10V. At voltage U=20V, when different sodium concentrations were added to xenon, the temperature decreased significantly from 1500 to 3000 K in plasma current density. The electric field is the reason for the increase in plasma current density this leads to increased collision and ionization processes.

Regarding the electron current density (je)) at U=10 V. At temperatures ranging from 3500 to 5000 K, electrons began to be emitted gradually. With increasing concentrations of sodium (0.001, 0.01, 0.1, and 0.5) mole, it is shown that the electron current density varies at temperatures ranging from (2600 to 5000) K. This is because there are more collisions and ionization processes, which increase the velocity of the electron. After all, the electron mobility at U=20 V was higher (Figures 1b, 2b, 3b, and 4b).

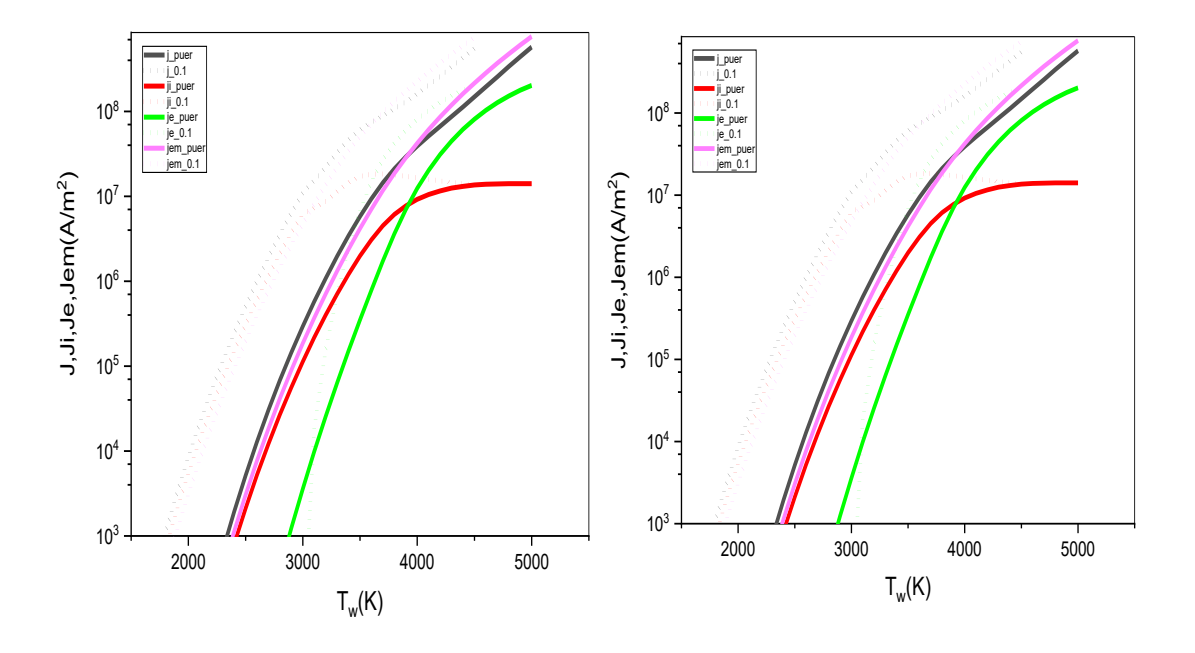
Regarding the ion current density  $(j_i)$  at U=10V, ions began to be emitted at temperatures (2400-5000) K. Different concentrations of sodium (0.001, 0.01, 0.1, and 0.5) mole caused an increase in ion emission as well as a shift in ion current density from 1500 to 5000 K. At U = 20V, for different sodium concentrations of (0.001, 0.01, 0.1 and 0.5) mole, an increase in electron emission processes was observed at (1400-5000) K. The increased ionization processes caused an increase in the release of ions from the cathode surface. Increased voltage U = 20 V caused an increase in the electric field and an increase in the current of ejected electrons.



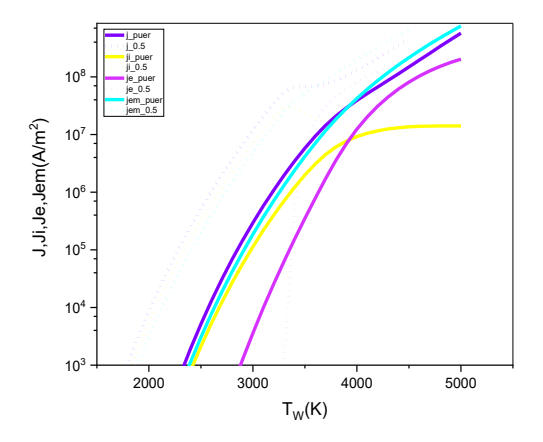
**Figure 2:** Current density j,  $j_e$ ,  $j_i$  and  $j_{em}$  vs cathode temperature at sodium concentration of 0.0001mole, at (a): U=10 V and (b): U=20V

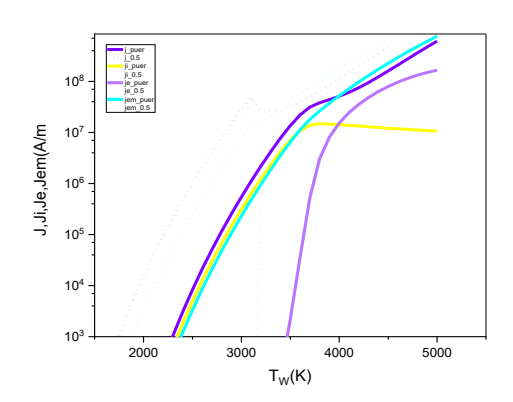


**Figure 3:** Current density j,  $j_e$ ,  $j_i$  and  $j_{em}$  vs cathode temperature at sodium concentration of 0.01mole, at (a): U=10 V and (b): U=20V



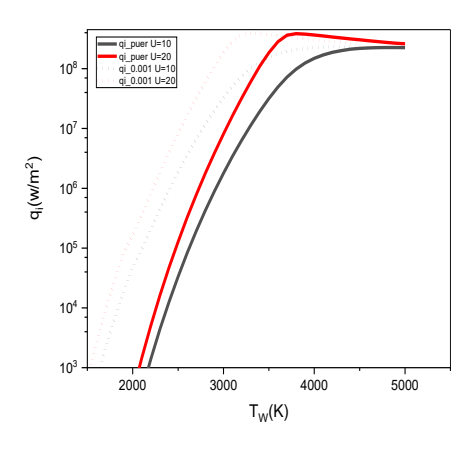
**Figure 4:** Current density j,  $j_e$ ,  $j_i$  and  $j_{em}$  vs. cathode temperature at sodium concentration of 0.1 mole, at (a): U=10 V and (b): U=20 V

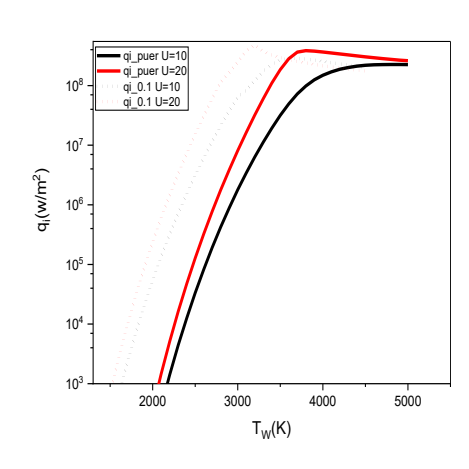


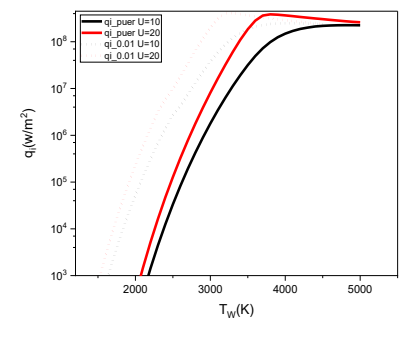


**Figure 5:** Current density j,  $j_e$ ,  $j_i$  and  $j_{em}$  vs. cathode temperature at sodium concentration of 0.5 mole, at (a): U=10 V and (b): U= 20 V

Figure (6) shows the relationship between the energy density of the ions (qi) and the temperature of the cathode surface (Tw) at applied voltages of U=10V and U=20V for different concentrations of sodium (0.001, 0.01, and 0.1) mole added to xenon. At U=10V, the ions started to emit at a temperature of (2200-5000) K due to collisions and the accumulated kinetic energy of ions. However, upon adding sodium with concentrations of (0.001, 0.01, and 0.1) mole, the energy density of the ions shifted, beginning from (1300-5000) K, as the ions' emission rose in tandem with the concentration and the potential difference at voltage U = 20V. Since a greater voltage produces a stronger electric field, this, in turn, causes ionization and excitation processes to intensify

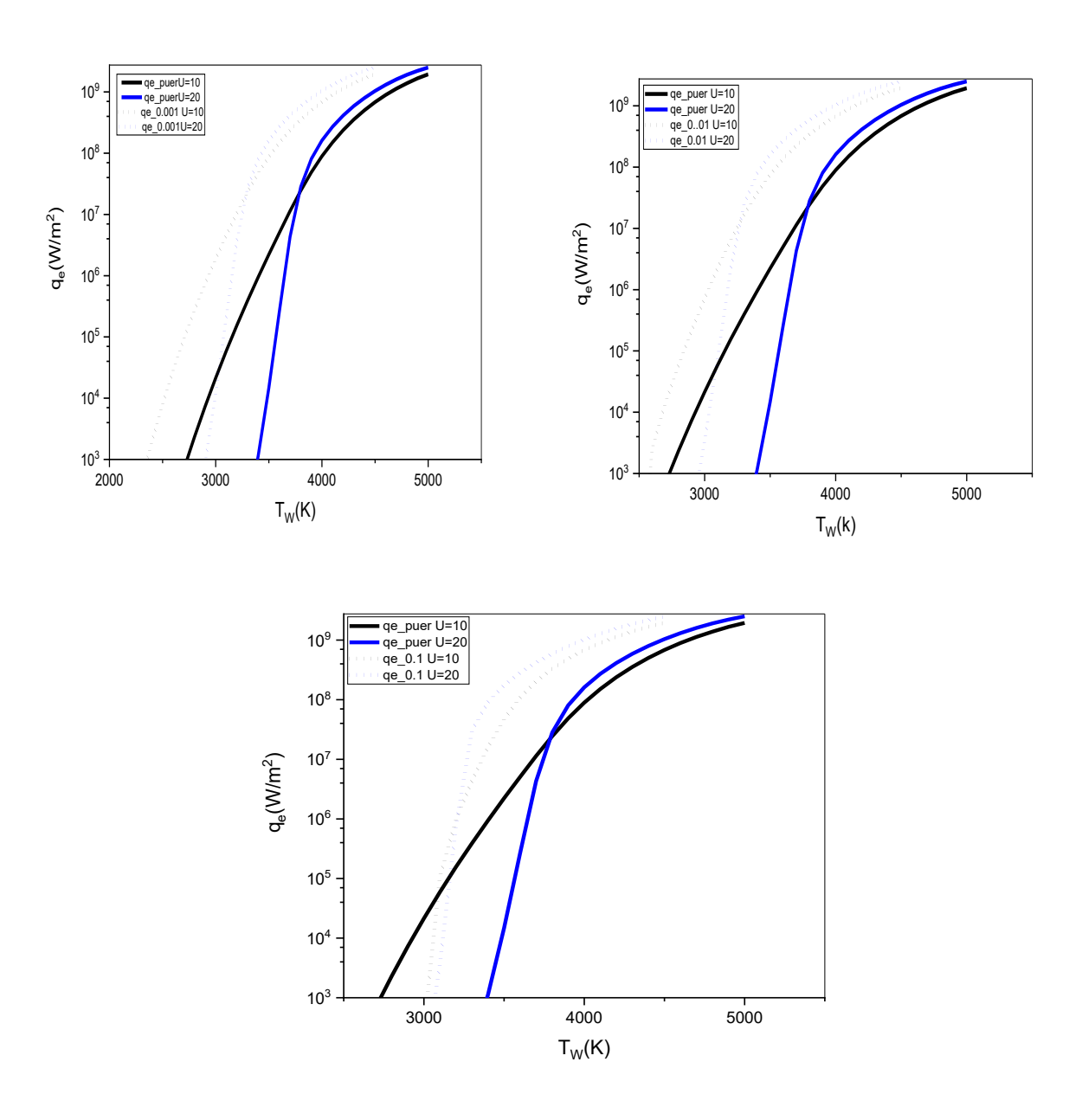






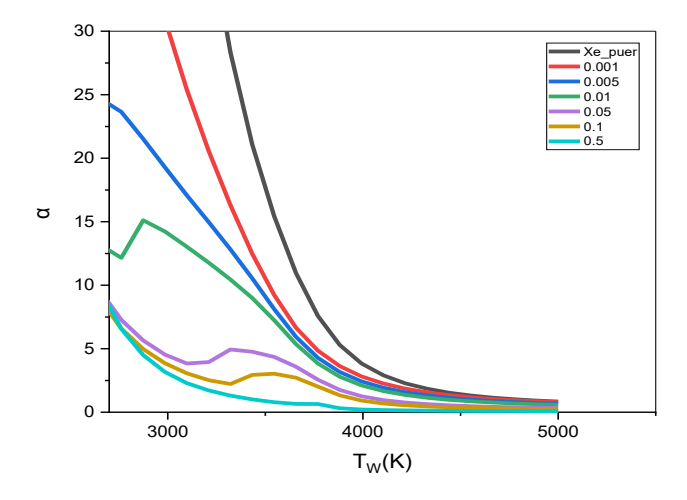
**Figure 6:** Energy density of the ions  $q_i$  vs. cathode temperature  $(T_w)$  at U=10 V and U=20V for (a) 0.001 mole, (b) 0.01 mole, and (c) 0.1 mole

Figure (7) shows the relationship between the ion energy density ( $q_i$ ) and the cathode surface temperature (Tw) at voltages of (U=10V and U=20V) for different sodium concentrations of (0.001, 0.01, and0.1) mole added to xenon. At U=10V, electrons began to be emitted at a temperature between 500 and 2500 K. When the voltage difference increased to 20 V, the average electron energy also increased and the electron energy density increased and began to be emitted at temperatures higher than 3800 K. This indicates that with increasing sodium concentrations added to xenon and increasing the applied voltage, a shift occurred at a lower temperature, which led to an increase in the electron density. This indicates that the electron energy density tends to expand with increasing voltage. Enhanced ionization processes provide more energy to the electrons, which increases the kinetic energy of the electron.



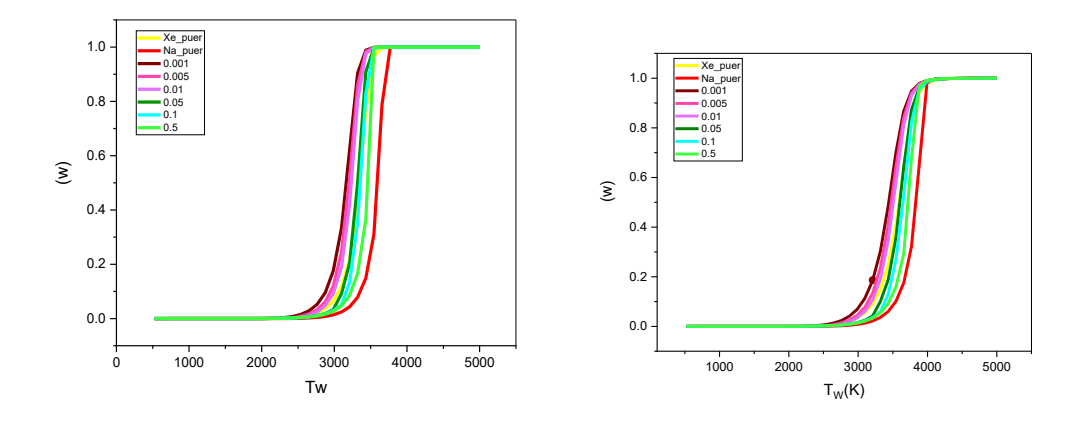
**Figure 7:** Energy density of electrons  $q_e$  vs. cathode temperature at U=10 V and U= 20 for (a) 0.001mole, (b) 0.01mole, and (c) 0.1mole

Figure (8) shows the ratio of ionization length to mean free path length ( $\alpha$ ) versus cathode temperature. Interactions between atoms of matter and ionizing particles are uncommon at very high concentrations of sodium (0.1 and 0.5) mole. This is due to the longer duration of particle impact at low temperatures, having a greater value for pure xenon and at a sodium concentration of 0.001 mole added to xenon. The ionization length decreased with increasing concentration at 0.1 and 0.5 mole because the particles collide more frequently at closer distances, leading to rapid ionization. This increase can be attributed to both the extension of the ionization process and the decrease in the mean free path length of the particle. Higher temperatures (4000-5000) K also decreased the mean free path  $\alpha$  of the particles because at higher temperatures, particles tend to move faster and are more likely to collide with each other. There may be more particle contacts and energy transfer as a result of the decreased mean free path.



**Figure 8:** Ratio of ionization length to mean free path  $\alpha$  vs. cathode temperature for all sodium concentrations at (a) U=10V and (b) U= 20V

As shown in Figure (9), when the temperature rises, the kinetic energy of the particles also rises, increasing the likelihood of collisions between the electrons and the particles and between the positively charged ions and the ionizing electrons. As can be seen from the figure, at U=10V, the degree of ionization started to increase at a temperature of 3000 K. The



**Figure 9:** Ionization degree vs. cathode temperature for all sodium concentrations at (a): U=10 V and (b): U=20 V

greatest level of ionization occurred at U=20V since as the voltage increases, so does the strength of the electric field inside the arc. This led to more collisions between atoms, neutral molecules, and electrons, which, in turn, increased the number of ionization events. The ionic strength may be altered by increasing the concentration of ions. An increase in ionic strength may cause the ions' activity coefficient to drop, which lowers the likelihood of ionizing the material. The mutual interference between ions and molecules caused by the high concentration making the ionization of the material more difficult, results in a reduction in the degree of ionization.

**Table 1:** The degree of ionization for the different sodium concentrations at the two voltages.

Concentrations	U=10 Volt	U= 20Volt
Xe_pure	$4.0 \times 10^{-1}$	$9.68 \times 10^{-1}$
Na_pure	$1.01 \times 10^{-1}$	$3.11 \times 10^{-1}$
0.001mole	$3.03 \times 10^{-1}$	$9.04 \times 10^{-1}$
0.005mole	$2.36 \times 10^{-1}$	$8.58 \times 10^{-1}$
0.01mole	$1.91 \times 10^{-1}$	$8.02 \times 10^{-1}$
0.05mole	$1.01 \times 10^{-1}$	$5.0 \times 10^{-1}$
0.1mole	$5.9 \times 10^{-2}$	$3.55 \times 10^{-1}$
0.5mole	$5.74 \times 10^{-2}$	$1.67 \times 10^{-1}$

#### **Conclusions**

By analysing the results, a direct proportionality was noticed between the ionization processes and the electric field, which led to an increase in the velocity of electrons due to the increase in the concentration of sodium (0.001, 0.01, 0.1 and 0.5 mole) added to the xenon. Also, the higher the temperature and the greater the concentration of sodium added to xenon, the greater the effect on each of  $(\alpha, \omega, j_p, j_i, j_e, j_{em}, , q_i \text{ and } q_e)$  as they increase due to the increase in elastic electron collisions and the increase in the kinetic energy of the internal electrons. The growth of electric field as a result of these changes in the density and concentration of electrons affected by the electric field is used in the manufacture of long-life arc discharge lamps that have a long life and long effective light emission.

#### 5. Acknowledgements

The authors would like to thank Mustansiriyah University (www.uomustansiriyah.edu.iq) Baghdad-Iraq for its support in the present work.

#### Reference.

- [1] M. T. Al-Obaidi, R. A. Ali, and B. Hamed, "Modelling of Reduced Electric Field and Concentration Influence on Electron Transport Coefficients of He-Ne Plasma.," *Acta Phys. Pol. A.*, vol. 140, no. 4, pp. 299-305, 2021.
- [2] A. A. Temur, A. F. Ahmed, and R. A. Ali, "Determination of the Mathematical Model for Plasma Electronic Coefficients of the Earth's Ionosphere," *Iraqi J. Sci.*, vol. 64, no. 3, pp. 1508–1517, 2023.
- [3] R. A. Ali, B. Hamed, M. T. Al-obaidi, and A. M. Abbas, "Estimation of a Mathematical Model for Theoretical Measuring of Plasma Electrons Mobility at Different Concentrations of He-Cu Mixture," in *Journal of Physics: Conference Series*, IOP Publishing, vol. 1999, p. 12132, 2021.
- [4] I. K. Abbas, "Influence of Distance and Argon Flow rate on Pseudomonas aeruginosa Bacteria Exposed to Non thermal Plasma at Atmospheric Pressure," *Iraqi J. Sci.*, vol. 63, pp. 4697–4704, 2022.
- [5] S. R. Choudhury and A. Goswami, "Non-metallic nanoparticles & their biological implications," *Basic Appl. Asp. Nanobiotechnology*, p. 61, 2017.

- [6] N. A. Timofeev, V. S. Sukhomlinov, G. Zissis, I. V Mukharaeva, and P. Dupuis, "Investigation of short-arc high-pressure xenon discharge: effect of electrode material evaporation on discharge properties and pulse operation," *IEEE Trans. Plasma Sci.*, vol. 47, no. 7, pp. 3266–3270, 2019.
- [7] G. Rego, "Fibre optic devices produced by arc discharges," J. Opt., vol. 12, no. 11, p. 113002, 2010.
- [8] S. Ghorui and A. K. Das, "Application of nonlinear dynamic techniques to high pressure plasma jets," *Journal of Physics: Conference Series*, IOP Publishing, vol. 208, p. 12057, 2010.
- [9] N. A. Timofeev, D. K. Solikhov, V. S. Sukhomlinov, and I. Y. Mukharaeva, "Investigation of a High-Pressure Short-Arc Xenon Discharge at Different Electrode Surface Shapes with Taking into Account Emission of Cathode Material into a Plasma," *High Energy Chem.*, vol. 57, no. Suppl 1, pp. S125–S131, 2023.
- [10] H. F. Jassam and R. A. Ali, "Interaction of near-cathode plasma layers with thermionic electrodes under high pressure arc plasma," in *Journal of Physics: Conference Series*, IOP Publishing, vol. 2322, p. 12076, 2022.
- [11] A. S. Noori, K. A. Aadim, and A. H. Hussein, "Investigate and Prepare silver Nano Particles Using Jet Plasma," *Iraqi J. Sci.*, vol. 63, pp. 2461–2469, 2022.
- [12] M. S. Benilov and S. Coulombe, "Modeling a collision-dominated space-charge sheath in high-pressure arc discharges," *Phys. Plasmas*, vol. 8, no. 9, pp. 4227–4233, 2001.
- [13] M. S. Benilov, N. A. Almeida, M. Baeva, M. D. Cunha, L. G. Benilova, and D. Uhrlandt, "Account of near-cathode sheath in numerical models of high-pressure arc discharges," *J. Phys. D. Appl. Phys.*, vol. 49, no. 21, p. 215201, 2016.
- [14] M. S. Benilov, M. D. Cunha, and G. V Naidis, "Modelling interaction of multispecies plasmas with thermionic cathodes," *Plasma Sources Sci. Technol.*, vol. 14, no. 3, p. 517, 2005.
- [15] M. S. Benilov, "Understanding and modelling plasma—electrode interaction in high-pressure arc discharges: a review," *J. Phys. D. Appl. Phys.*, vol. 41, no. 14, p. 144001, 2008.
- [16] A. Javidi-Shirvan, Modelling of Cathode-Plasma Interaction in Short High-Intensity Electric Arc—Application to Gas Tungsten Arc Welding. Chalmers Tekniska Hogskola (Sweden), 2016.
- [17] M. S. Benilov and M. D. Cunha, "Heating of refractory cathodes by high-pressure arc plasmas: I," *J. Phys. D. Appl. Phys.*, vol. 35, no. 14, p. 1736, 2002.
- [18] M. A. Lieberman, "Plasma discharges for materials processing and display applications," *Adv. Technol. Based Wave Beam Gener. Plasmas*, vol. 67, pp. 1–22, 1999.
- [19] I. I. Beilis, "Plasma Energy Loss by Cathode Heat Conduction in a Vacuum Arc: Cathode Effective Voltage," *Plasma*, vol. 6, no. 3, pp. 492–502, 2023.
- [20] A. Trník and L. Vozár, "Modeling of heat capacity peaks and enthalpy jumps of phase-change materials used for thermal energy storage," *Int. J. Heat Mass Transf.*, vol. 107, pp. 123–132, 2017.